JOURNAL OF AIRCRAFT
Vol. 48, No. 4, July–August 2011

Flutter Analysis of Aerostructures Test Wing with Test Validated Structural Dynamic Model

Chan-gi Pak* and Shun-fat Lung†
NASA Dryden Flight Research Center, Edwards, California 93523-0273

DOI: 10.2514/1.C031257

Tuning a finite element model using measured data to minimize the model uncertainties is a challenging task in the area of structural dynamics. A test-validated finite element model can provide a reliable flutter analysis to define the flutter placard speed to which the aircraft can be flown before flight flutter testing. Minimizing the difference between numerical and experimental results is a type of optimization problem. Through the use of the NASA Dryden Flight Research Center's multidisciplinary design, analysis, and optimization tool to optimize the objective function and constraints, the mass properties, natural frequencies, and mode shapes are matched to the target data and the mass matrix orthogonality is retained. The approach in this study has been applied to minimize the model uncertainties for the structural dynamic model of the Aerostructures Test Wing, which was designed, built, and tested at the NASA Dryden Flight Research Center. A 25% change in flutter speed has been shown after reducing the uncertainties. Therefore, without reducing the uncertainties, 40% of the flutter margin (15% MIL-SPEC requirement + 25% modeling uncertainties) would be needed for the safety of flight test.

Nomenclature

d	=	number of degrees of freedom
F	=	original objective function
G	=	subscript for target values (or measured quantities)
g_i	=	inequality constraints
h_i	=	equality constraints
I_{XX}	=	computed x moment of inertia about center of gravity
I_{YY}	=	computed y moment of inertia about center of gravity
I_{ZZ}	=	computed z moment of inertia about center of gravity
J_i	=	objective functions (Optimization problem statement number $i = 1, 2, \ldots, 13$)
$\mathbf{K}$	=	stiffness matrix
$\bar{\mathbf{K}}$	=	orthonormalized stiffness matrix
L	=	new objective function
l	=	number of modes
$\mathbf{M}$	=	mass matrix
$\bar{\mathbf{M}}$	=	orthonormalized mass matrix
m	=	number of sensors (or number of measured degrees of freedom)
n	=	number of modes to be matched
q	=	number of inequality constraints
r	=	number of equality constraints
$\mathbf{T}$	=	transformation matrix
W	=	computed total mass
X	=	x-coordinate of computed center of gravity
$\bar{X}$	=	design variables vector
Y	=	y-coordinate of computed center of gravity
Z	=	z-coordinate of computed center of gravity
ε	=	small tolerance value for inequality constraints
λ	=	Lagrange multiplier
$\mathbf{\Phi}$	=	computed eigenmatrix ($m \times n$)
Ω_j	=	j-th computed frequency

Received 1 October 2010; revision received 26 January 2011; accepted for publication 25 February 2011.

*Structural Dynamics Group, Aerostructures Branch. Senior Member AIAA.

†Contractor, Tybrin Corporation. Member AIAA.

I. Introduction

A TEST article called the Aerostructures Test Wing (ATW) was developed and flown at the NASA Dryden Flight Research Center (DFRC) on the F15B test bed aircraft, as shown in Fig. 1, to demonstrate and validate flutter prediction methods during flight [1]. The first Aerostructures Test Wing (ATW1) was developed in 2001 to address requests for better flight flutter test techniques by providing a functional flight-test platform. While the first series of tests was extremely successful, the minimum amount of instrumentation (structural accelerometers and strain gages) was chosen to satisfy the scope of the program. These sensors were limited in the capability to answer questions of aeroelastic interactions, sources of nonlinearity, physical mechanisms of aeroelastic coupling, and feedback dynamics between the structure and aerodynamics.

A second Aerostructures Test Wing (ATW2), as shown in Fig. 2, has been built to demonstrate state-of-the-art sensor technologies for simultaneous, distributed, and collocated measurement of shear stress (skin friction); steady and unsteady pressures; and structural strain and accelerations for mode shapes and other modal properties. This wing was flown on the F15B on 15 December 2009. The ATW1 and ATW2 had the same wing geometries and cross-sectional shapes. These two wings were constructed based on the same design specifications. However, the major difference between the ATW1 and ATW2 was the composite construction and mass balancing. The ATW1 and ATW2 were built by two different vendors, and had different type of piezo patches at different locations. In case of the ATW1, the boom end-caps contained powdered tungsten for mass balancing to increase the flutter speed. These mass balancing were omitted for the ATW2.

A block diagram for a flutter analysis procedure used at NASA DFRC is given in Fig. 3. Using a finite element (FE) model for a structural dynamic analysis becomes increasingly important in the modern aircraft design and analysis processes. However, the quality of an initial FE model of an aircraft is not guaranteed, so we need to perform the ground vibration test (GVT) to validate the FE model. In most cases, these newly built FE models need to be tuned to minimize uncertainties in the structural dynamic FE models and flutter boundary results. Flutter analyses performed at NASA DFRC are mainly based on these validated FE models as shown in Fig. 3.

Model tuning is a common method to improve the correlation between numerical and experimental modal data, and many techniques have been proposed [2]. Literature reviews on FE model tuning are summarized in the [3]. These techniques can be divided into two categories: direct methods (adjusting the mass and stiffness matrices directly) and parametric methods (correcting the models by

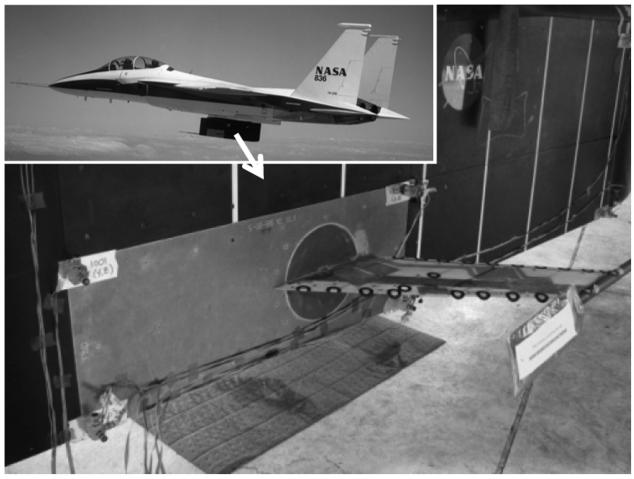

Fig. 1 Aerostructures test wing mounted on F15B for the flight flutter testing.

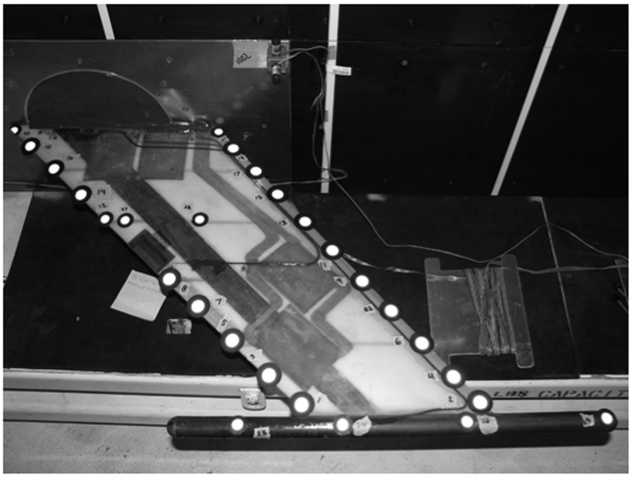

Fig. 2 Aerostructures test wing 2.

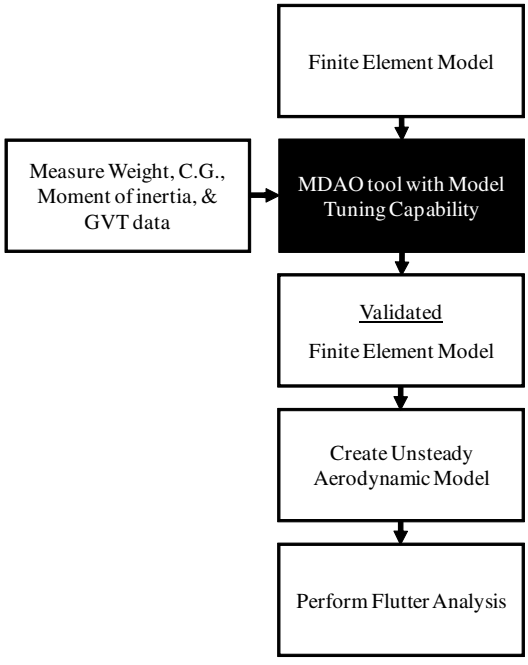

Fig. 3 Flutter analysis procedure at NASA DFRC.

changing the structural parameters). The direct methods correct mass and stiffness matrices without taking into account the physical characteristics of the structures and may not be appropriate for use in model tuning processes. In this paper, the tuning method used in the optimization process is the parametric method. In the optimization process, structural parameters are selected as design variables: structural sizing information (thickness, cross-sectional area, area moment of inertia, torsional constant, etc.), point properties (lumped mass, spring constants, etc.) and materials properties (density, Young's modulus, etc.). Objective function and constraint equations include mass properties, mass matrix orthogonality, frequencies, and mode shapes. The use of these equations minimizes the difference between numerical results and target data.

The primary objective of this study is to reduce uncertainties in the structural dynamic FE model of the ATW2 to increase the safety of flight. Discrepancies are common between the test data and numerical results. However, the FE model can be fine tuned through the use of GVT data. Accurate and reliable GVT results are important to this adjusting process.

The secondary objective of the current study is to add model tuning capabilities [3] in NASA DFRC's object-oriented multidisciplinary design, analysis and optimization (MDAO) tool [4]. This model tuning technique [3] is essentially based on a nonlinear optimization problem.

II. Object-Oriented MDAO Framework

The heart of the object-oriented MDAO tool is the central executive module (CEM) as shown in Fig. 4. In this module the user will choose an optimization methodology, provide side constraints for continuous as well as discrete design variables and external file names for performance indices, which communicate between the CEM and each analysis module, submit script commands to prepare input data for each analysis code, execute analyses codes, compute performance indices using postprocessor codes, and compute an objective function and constraints values from performance indices. The CEM was written in FORTRAN and script commands for each performance index were submitted through the use of the FORTRAN "call system" command.

The performance indices for structural optimization problems can include total weight, safety factors, natural frequencies, mode shapes, flutter speed, divergence speed, structural responses at sensor locations, etc. On the other hand, the performance indices for the FE model tuning problems can include off-diagonal terms of orthonormalized mass and stiffness matrices, the total error between the measured and computed mode shapes at given sensor points, errors between computed and measured frequencies, total weight, center of gravity (c.g.) locations, moment of inertia, etc.

Two external optimization codes are included in the object-oriented MDAO tool: design optimization tools (DOTs) [5] based on a gradient-based algorithm [6] and a genetic algorithm (GA) [7]. MSC/NASTRAN, for example, uses a gradient-based approach for optimization [8]. A drawback to this approach is the necessity to compute finite difference or analytical sensitivity values to perform the search, which often requires prior experience based on input defining the problem and search directions.

DOT is a commercial optimization code that can be used to solve a wide variety of nonlinear optimization problems. When DOT requires the values of the objective and constraint functions corresponding to a proposed design, it returns control to the CEM. The CEM calls DOT again to obtain the next design point. This process is repeated until DOT returns a parameter to indicate that the optimum objective function is reached. Gradient-based algorithms work well for continuous design variable problems, whereas GAs can easily handle continuous as well as discrete design variable problems. When there are multiple local minima, GAs are able to find the global optimum results, whereas gradient-based methods may converge to a locally minimum value.

The GA is directly applicable only to unconstrained optimization so it is necessary to use some additional methods to solve the constrained optimization problem. The most popular approach is to

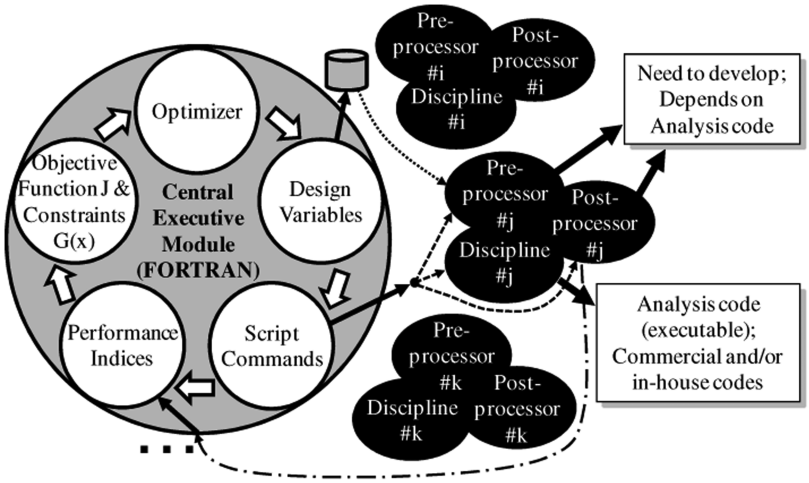

Fig. 4 Central executive module.

add penalty functions, in proportion to the magnitude of the constraint violation, to the objective function [9].

The general form of the exterior penalty function is shown in Eq. (1):

$$\mathbf{L}(\bar{\mathbf{X}}) = \mathbf{F}(\bar{\mathbf{X}}) + \sum_{i=1}^{q} \lambda_i \mathbf{g}_i(\bar{\mathbf{X}}) + \sum_{j=1}^{r} \lambda_{j+q} \mathbf{h}_j(\bar{\mathbf{X}}) \tag{1}$$

where $\mathbf{L}(\bar{\mathbf{X}})$ indicates the new objective function to be optimized, $\mathbf{F}(\bar{\mathbf{X}})$ is the original objective function, $\mathbf{g}_i(\bar{\mathbf{X}})$ is the inequality constraint, $\mathbf{h}_j(\bar{\mathbf{X}})$ is the equality constraint, λ_i are the scaling factors, $\bar{\mathbf{X}}$ is the design variables vector, and q and r are the number of inequality and equality constraints, respectively.

Five optimization methodologies available in the CEM are described as follows: 1) genetic algorithm with continuous, discrete or mixed (continuous/discrete) design variables (GCD); 2) gradient-based algorithm, that is DOT, with continuous design variables (DC); 3) start with GCD then continue with DC; 4) start with GCD then continue with DC then continue with genetic algorithm with discrete design variables (GD); and 5) start with DC then continue with GD.

III. Structural Dynamic Model Tuning Procedure

Discrepancies in frequencies and mode shapes are minimized using a series of optimization procedures [3,10,11]. The numerical mass properties, the mass matrix orthogonality, and the natural frequencies and mode shapes are matched to the target values based on the following three tuning steps.

A. Step 1: Tuning Mass Properties

The difference in the numerical and target values of the total mass, the c.g. location, and mass moment of inertias at the c.g. location are used as performance indices. The resulting 10 performance indices, as shown in Eqs. (2–11), are defined to minimize the uncertainties in the rigid body dynamics:

$$J_1 = (W - W_G)^2 / W_G^2 \qquad \text{(Total weight)} \tag{2}$$

$$J_2 = (X - X_G)^2 / X_G^2 \qquad (X\text{-CG location}) \tag{3}$$

$$J_3 = (Y - Y_G)^2 / Y_G^2 \qquad (Y\text{-CG location}) \tag{4}$$

$$J_4 = (Z - Z_G)^2 / Z_G^2 \qquad (Z\text{-CG location}) \tag{5}$$

$$J_5 = (I_{XX} - I_{XXG})^2 / I_{XXG}^2 \qquad (I_{XX} \text{ at CG}) \tag{6}$$

$$J_6 = (I_{YY} - I_{YYG})^2 / I_{YYG}^2 \qquad (I_{YY} \text{ at CG}) \tag{7}$$

$$J_7 = (I_{ZZ} - I_{ZZG})^2 / I_{ZZG}^2 \qquad (I_{ZZ} \text{ at CG}) \tag{8}$$

$$J_8 = (I_{XY} - I_{XYG})^2 / I_{XYG}^2 \qquad (I_{XY} \text{ at CG}) \tag{9}$$

$$J_9 = (I_{YZ} - I_{YZG})^2 / I_{YZG}^2 \qquad (I_{YZ} \text{ at CG}) \tag{10}$$

$$J_{10} = (I_{ZX} - I_{ZXG})^2 / I_{ZXG}^2 \qquad (I_{ZX} \text{ at CG}) \tag{11}$$

In case of DOT optimization, it is recommended to start an optimization procedure at a feasible domain. When the optimization procedure starts in an infeasible domain, there is no guarantee that the design will move to a feasible domain. To this end, these 10 sub-optimization criteria are used (if test data is available) to make a feasible starting configuration for the second and the third optimization steps.

The exterior penalty function approach given in Eq. (1) is used for the GA optimization. For example, the performance index J_1 selected as an objective function and performance indices J_2 through J_{10} as constraints, then the following objective function J can be used for the GA optimization as shown in Eq. (12)

$$J = J_1 + \sum_{i=2}^{10} \lambda_i J_i \tag{12}$$

where λ_i is the scaling factors and $i = 2, \ldots, 10$.

B. Step 2: Tuning Mass Matrix

The off-diagonal terms of the orthonormalized mass matrix are reduced to improve the mass orthogonality as shown in Eq. (13):

$$\mathbf{J}_{11} = \sum_{i=1, j=1, i \neq j}^{n} (\bar{\mathbf{M}}_{ij})^2 \tag{13}$$

where n is the number of modes to be matched and $\bar{\mathbf{M}}$ is defined as shown in Eq. (14)

$$\bar{\mathbf{M}} = \mathbf{\Phi}_G^T \mathbf{T}^T \mathbf{M} \mathbf{T} \mathbf{\Phi}_G \tag{14}$$

The performance index J_{11} is used as the objective function and performance indices J_1 through J_{10} are used as constraints in this step. In Eq. (14), the mass matrix $\mathbf{M}$ is calculated from the FE model while the target eigenmatrix $\mathbf{\Phi}_G$ is measured from the GVT. The eigenmatrix $\mathbf{\Phi}_G$ remains constant during the optimization procedure. A transformation matrix $\mathbf{T}$ [3] in Eq. (14) is based on Guyan reduction, improved reduction system [12] or system equivalent reduction expansion process [13]. This reduction is required due to

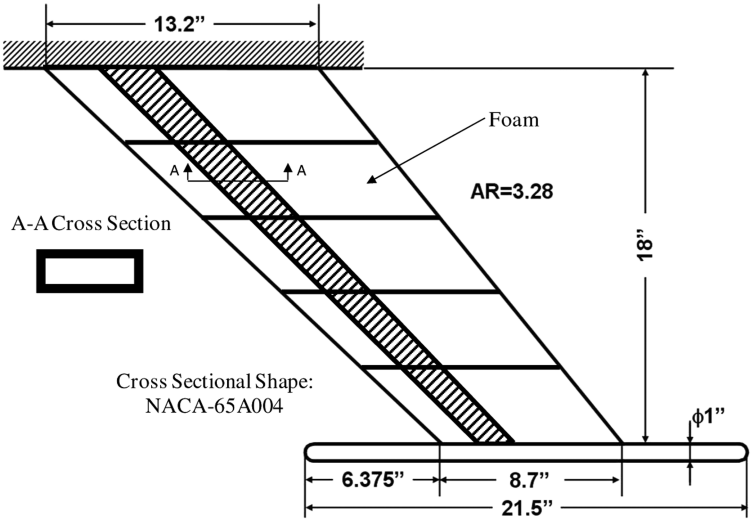

Fig. 5 Exploded view of the ATW2.

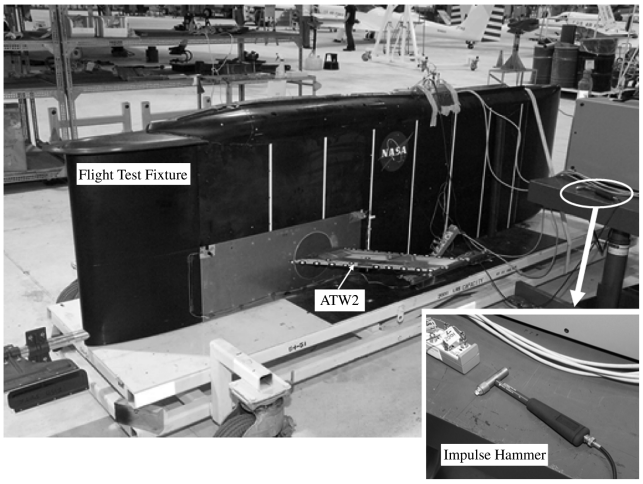

Fig. 6 Fight-test fixture and ATW2 on ground handling cart.

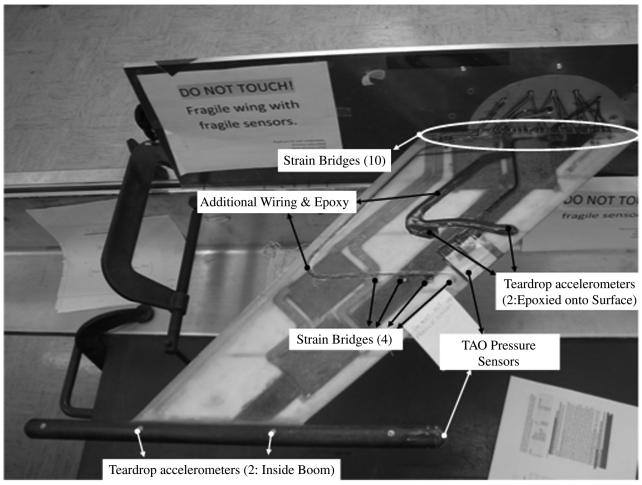

Fig. 7 Bottom view of the ATW2 with instrumentation call-outs.

the limited number of available sensor locations and difficulties in measuring the rotational DOFs.

C. Step 3: Tuning Frequencies and Mode Shapes

Two options can be used for tuning the frequencies and mode shapes. In the first option, the objective function considered combines a performance index J_{12} (the normalized errors between GVT and computed frequencies) as shown in Eq. (15) with a performance index J_{13} (the total error associated with the off-diagonal terms of the orthonormalized stiffness matrix) as shown in Eq. (16)

$$\mathbf{J}_{12} = \sum_{i=1}^{n} \left(\frac{\boldsymbol{\Omega}_i - \boldsymbol{\Omega}_{iG}}{\boldsymbol{\Omega}_i} \right)^2 \tag{15}$$

$$\mathbf{J}_{13} = \sum_{i=1,j=1,i\neq j}^{n} (\bar{\mathbf{K}}_{ij})^2 \qquad \text{(option 1)} \tag{16}$$

The matrix $\bar{\mathbf{K}}$ is obtained from the following matrix products as shown in Eq. (17):

$$\bar{\mathbf{K}} = \boldsymbol{\Phi}_G^T \mathbf{T}^T \mathbf{K} \mathbf{T} \boldsymbol{\Phi}_G \tag{17}$$

where the stiffness matrix $\mathbf{K}$ is calculated from the FE model.

In the second option, the objective function considered combines the performance index J_{12} with a new performance index J_{13} (the total error between GVT and computed mode shapes at given sensor points) as shown in Eq. (18)

Table 1 Natural frequencies of the ATW2 before and after model tuning

Mode	GVT				Before tuning			After tuning		
	#2 with FTF		#3 with FTF and F15B		Frequency, Hz ([16,17])	Error		Frequency, Hz	Error	
	Frequency, Hz	Damping, %	Freqency, Hz	Damping, %		With respect to #2, %	With respect to #3, %		With respect to #2, %	With respect to #3, %
1	17.45	0.623	17.42	0.575	17.60	0.86	1.03	17.45	0.00	0.17
2	43.72	0.610	43.73	0.643	23.26	−46.8	−46.8	43.48	−0.55	−0.57
3	83.66	0.778	84.14	0.724	93.99	12.4	11.7	82.98	−0.81	−1.38
4	——	——	——	——	135.4	——	——	133.6	——	——
5	142.3	0.674	143.0	0.694	163.1	14.6	14.1	153.8	8.08	7.55

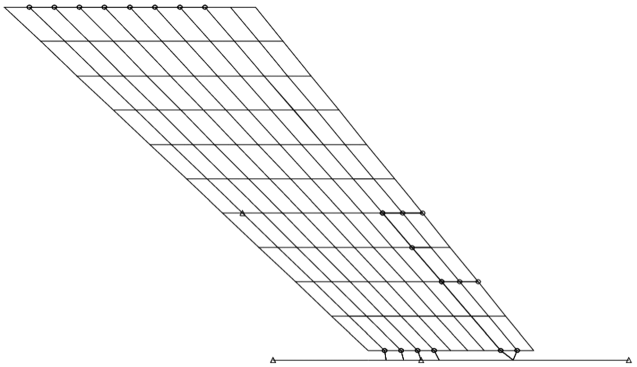

Fig. 8 MSC/NASTRAN finite element model.

$$\mathbf{J}_{13} = \sum_{i=1}^{m}\sum_{j=1}^{n}(\mathbf{\Phi}_{ij} - \mathbf{\Phi}_{ijG})^2 \qquad \text{(option 2)} \qquad (18)$$

The performance index J_{13}, in the second option, is much simpler than in the first option for this application. Any errors in both the modal frequencies and the mode shapes are minimized by including an index for each of these in the objective function. For the second option, a small number of sensor locations can be used at which errors between the GVT and computed mode shapes are obtained.

Instead of using the summation in Eqs. (13) and (15), each individual term can be a separate performance index. In this case, total number of performance indices for the steps 2 and 3 will increase; however, it is easier to apply the military standard requirements, the frequency error should be less than 3% for the primary modes and 10% for the secondary modes [14,15].

Any one or combinations of performance indices J_1 through J_{13} can be used as the objective function with the other performance indices treated as constraints. This gives the flexibility to achieve the particular optimization goal while maintaining the other properties as close to the desired target value as possible. The optimization problem statement can be written as

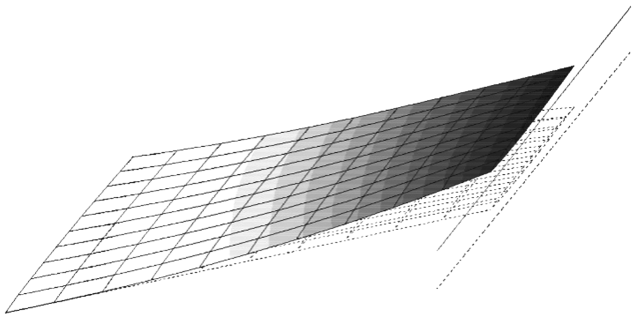

a) Mode 1 (1st bending): 17.60 Hz

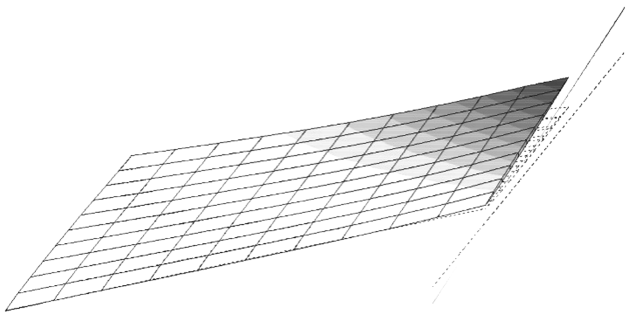

b) Mode 2 (1st torsion): 23.26 Hz

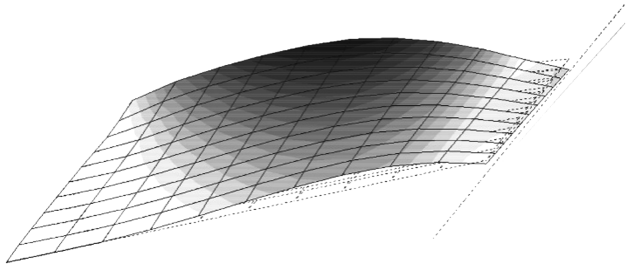

c) Mode 3 (2nd bending): 93.99 Hz

Fig. 9 Full model mode shapes before tuning.

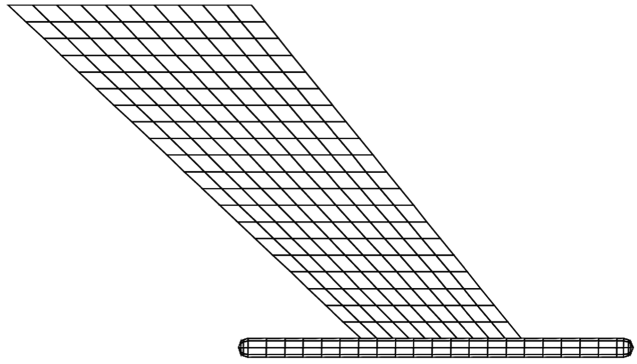

Fig. 10 ZAERO unsteady aerodynamic model.

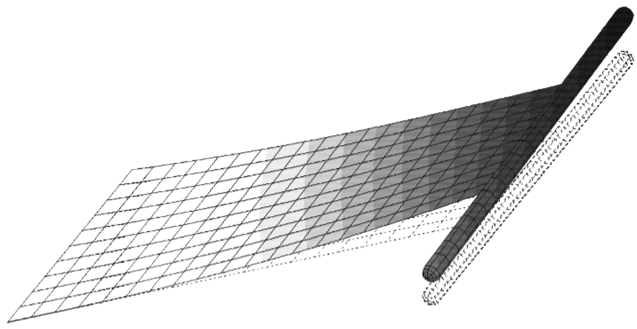

a) Splined mode 1

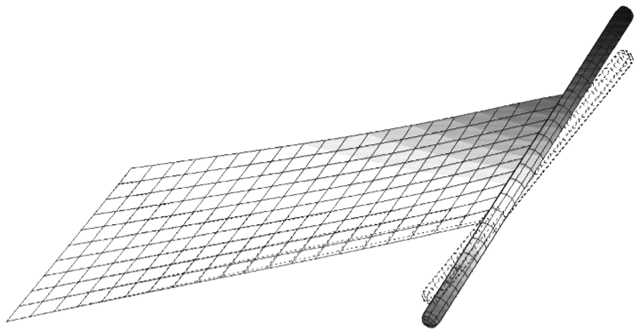

b) Splined mode 2

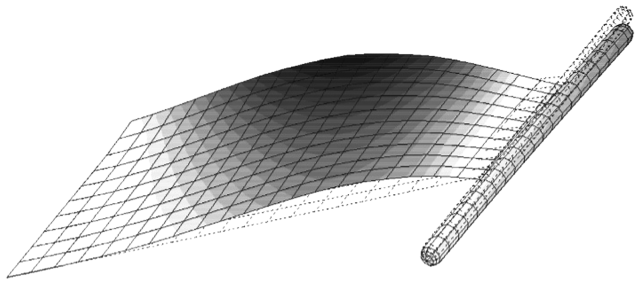

c) Splined mode 3

Fig. 11 Splined mode shapes on unsteady aerodynamic model.

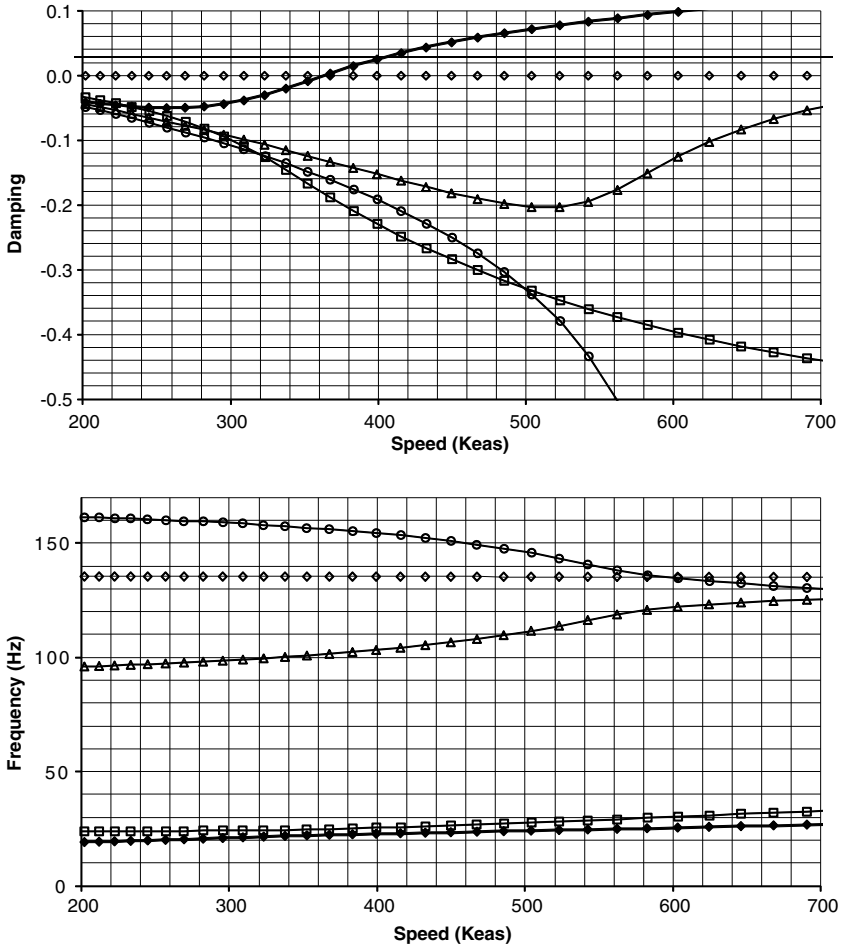

Fig. 12 *V-g* and *V-ω* plots for the ATW2 at Mach 0.82 before model tuning (plot the first five modes).

$$\text{Minimize } J_i$$

$$\text{such that } J_k \le \varepsilon_k, \quad \text{for } k = 1 \text{ through } 13 \text{ and } k \ne i$$

where ε_k is a small value that can be adjusted according to the tolerance of each constraint condition.

IV. Test Article

We use the ATW2 to demonstrate NASA DFRC's object-oriented MDAO tool through the process of ground vibration testing and the model tuning technique. This test article was a small-scale airplane wing composed of an airfoil and wing-tip boom as shown in Fig. 5. This wing had a major composite spar with a rectangular cross section, four equally spaced ribs, and composite upper and lower cover skins. Plastic foam was used to fill the empty space between the upper and the lower cover skins. This wing was based on a NACA-65A004 airfoil shape with a 3.28 aspect ratio, a −3° washout at the tip, and a 45° aft sweep angle at quarter chord. The total area of the ATW2 was 197 square inches with a half span of 18 in., a root chord length of 13.2 in., and a tip chord length of 8.7 in. The wing-tip boom was a 1-in. diameter hollow tube of 21.5 in. in length and the total weight of the wing was 2.66 lbs.

Since the ATW2 was attached to the F15B flight-test fixture (FTF), the construction of the wing was limited to lightweight materials with no metal for the safety of recontact with the aircraft after a possible separation. The wing and spar were constructed from fiberglass cloth, the tip boom used carbon fiber composite, the wing core consisted of rigid foam, and the components were attached by epoxy. The wing skin was made of three plies of fiberglass cloth with a 0.01 in. thickness. The internal spar located at the 30% chord line was composed of 10 plies with a 0.05 in. thickness of carbon at the root, and decreasing to 1 ply 0.005 in. thickness at the tip.

V. Test Setup

A FE model for the ATW2 has been created and updated to match the modal results of the first GVT. The FE model as well as the measured and numerical modal frequencies and mode shapes are given in [16,17].

Since the first GVT, additional flight instrumentation, associated wiring, and protective coatings have been added to the structure.

Table 2 Flutter boundaries before and after model tuning

		Mach = 0.60	Mach = 0.75	Mach = 0.82	Mach = 0.95
Before tuning	Speed, Keas	453.0	421.5	407.4	377.9
	Frequency, Hz	23.18	22.97	22.86	22.53
	Altitude, ft	−7501	8751	15010	25590
After tuning	Speed, Keas	337.9	340.5	341.5	344.7
	Frequency, Hz	35.96	35.11	34.59	32.91
	Altitude, ft	8642	19400	23475	29700
Speed error, %		33.8	23.8	19.3	9.6

Table 3 Modal participation factors at Mach 0.82 before model tuning

Mode	Frequency, Hz	Modal participation factor, %	
1	17.60	75.0	
2	23.26	16.8	96.6[a]
3	93.99	4.8	
4	135.4	0.0	
5	163.1	2.6	
6	174.5	0.0	
7	257.5	0.5	3.4[b]
8	391.6	0.0	
9	394.3	0.1	
10	445.6	0.3	

[a]The total of the first three modes.
[b]The total of the modes 5, 7, 9, and 10.

These additions have changed the mass properties of the wing, therefore requiring a new validation of the FE model. The second GVT was performed while the ATW2 was mounted to the FTF in the FTF ground handling cart, as shown in Fig. 6, and the third GVT was performed while ATW2/FTF were attached to the F15B centerline pylon, as shown in Fig. 1.

The ATW2 with all current instrumentation, for the second and third GVTs, is shown in Fig. 7. Installed instrumentation includes 14 total strain bridges (10 near the wing root and 4 along the midspan); TAO systems' hot-film sensors in two locations (over the leading edge near midspan and on the leading tip of the boom); 4 PCB 352C22 teardrop accelerometers (2 located within the wing-tip boom and 2 permanently installed on the bottom surface of the wing near the leading-edge hot-film sensor); and associated wiring. For the excitation method, an impulse hammer with an impedance head, as shown in Fig. 6, was used to excite the natural frequencies and mode shapes of the ATW2 as well as to measure input forces.

VI. Flutter Analysis Before Model Tuning

Natural frequencies obtained from the second and third GVTs and MSC/NASTRAN modal analyses using FE models before and after model tuning are summarized in Table 1. The starting configuration of the FE model was obtained from the ATW1 model. The software used to acquire data and to identify the frequencies and mode shapes of the system was the I-DEAS modal and signal processing modules. The FE model for MSC/NASTRAN [18] modal analysis is shown in Fig. 8. Detailed GVT sensor locations and GVT mode shapes are provided in the [16]. Corresponding natural frequencies and mode shapes computed using MSC/NASTRAN code are shown in Fig. 9. In Table 1 and Fig. 9, the mode numbers 1, 2, and 3 are the first bending, first torsion, and second bending, respectively. Mode numbers 4 and 5 in Table 1 are the in-plane wing bending and second bending/first torsion modes, respectively.

A matched flutter analysis of the ATW2 using ZAERO code [19] is presented in this section. The first 10 natural modes were used for the flutter analysis. The aerodynamic model has 200 surface elements on the wing and 216 body elements on the boom. Forty-four splining points were used between the structural dynamic and aerodynamic models. The aerodynamic model of the ATW2 and the first three splined mode shapes on the aerodynamic model are shown in Figs. 10 and 11, respectively. The matched flutter analyses were performed at 4 Mach numbers, 0.60, 0.75, 0.82, and 0.95. The aerodynamic influence coefficient matrices at each Mach number were generated at 16 reduced frequencies and the g-method [19] was used in the matched flutter analysis.

The speed versus damping V-g and speed versus frequency V-ω curves from the matched flutter analysis at Mach 0.82 (the ATW1 flutter Mach number [1]) before model tuning are given in Fig. 12. The structural damping used for the flutter speed computation was 3%. The flutter speed was 407.4 KEAS, flutter frequency was 22.86 Hz and the corresponding altitude was 15,010 ft, as shown in Table 2.

Modal participation factors for the first flutter mode are given in Table 3. Modal participation of the first three natural frequencies was more than 96% before model tuning. In-plane modes, mode numbers 4, 6, and 8, did not contribute to the first flutter mode. In Table 3, we can conclude that the primary structural dynamic modes for the first flutter mode were modes 1, 2, and 3 and the secondary modes for the first flutter mode were modes 5, 7, 9, and 10. The first mode is the dominant mode for the primary flutter mode.

VII. Model Tuning

Using a norm of the first three frequency differences as an objective function and mass properties, mass orthogonality and mode shapes as constraint equations, the frequencies after model tuning are presented in Table 1. The second GVT data, configuration with the FTF and without the F15B, was used as the target frequencies and mode shapes during the structural model tuning procedure.

Before model tuning, the frequency error for the second mode was 46.8/46.8% and the frequency error for the third mode was 12.4/11.7% , with respect to the second and third GVT data, respectively. These frequency errors violate the 3% frequency error requirements in military standards. After model tuning, the 0.86/46.8/12.4% error becomes 0.00/0.55/0.81% compared with the second GVT data. On the other hand, the 1.03/46.8/11.7% error becomes 0.17/0.57/1.38% compared with the third GVT data. After model tuning, 3% frequency error requirements for the first three primary modes were all satisfied and the 10% frequency error requirements for the secondary modes were also satisfied, as shown in Table 1. Therefore, the FE model tuned using the second GVT data was used for the flutter analysis of the final configuration, i.e., the third GVT configuration.

Table 4 shows the total weight, orthonormalized mass matrix, and modal assurance criterion (MAC) [3] values of the ATW2 before and after model tuning. The total weight of 2.66 lb in this table was measured during the first GVT [17]. The total weight of the ATW2 was increased due to the effect of 14 strain bridges, two TAO systems' hot-film sensors, four PCB 352C22 teardrop

Table 4 Summary of total weight, orthonormalized mass matrix, and MAC values for the ATW2 before and after model tuning (the second GVT data were used)

	Measured	Before tuning			After tuning		
Total weight	2.66 lb[a]	1.76 lb (error 34%)			2.85 lb (error 7.1%)[b]		
		1	2	3	1	2	3
Orthonormalized mass matrix	1	1	−0.249	0.380	1	−0.0192	−0.0446
	2	−0.249	1	−0.661	−0.0192	1	0.0616
	3	0.380	−0.661	1	−0.0446	0.0616	1
MAC	Mode 1		.97			.99	
	Mode 2		.70			.99	
	Mode 3		.75			.98	

[a]Measured using the first GVT configuration
[b]Weight of the wing was increased due to the effect of 14 strain bridges, two TAO systems' hot-film sensors, four PCB 352C22 teardrop accelerometers, and associated wiring.

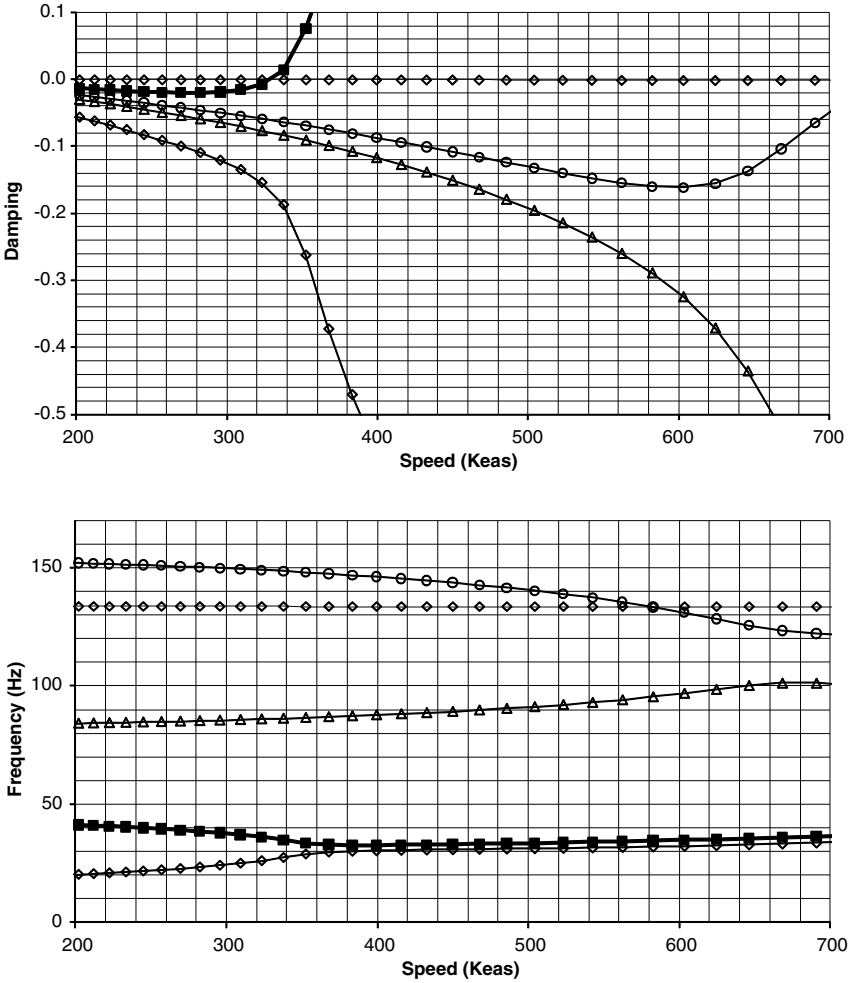

Fig. 13 *V-g* and *V-ωω* plots for the ATW2 at Mach 0.82 after model tuning (plot the first five modes).

accelerometers, and associated wiring as shown in Fig. 7. Weight of these additional sensors and wires were not measured.

Based on military standards, the off-diagonal terms of the orthonormalized mass matrix should be less than 10% [14,15]. The off-diagonal terms of the orthonormalized mass matrix, with a maximum of 66.1% before model tuning, are minimized in the second tuning step. The maximum off-diagonal term of 6.16% after model tuning is observed in Table 4 and satisfies the 10% limitation in military standards. Model correlation with the second GVT data before model tuning was poor and unacceptable to proceed to flight. The MAC values of 0.70 and 0.75 for modes 2 and 3 before model tuning become 0.99 and 0.98, respectively. Therefore, we can conclude that excellent model correlation with the test data was achieved after model tuning, which leads to a more reliable flutter speed prediction.

VIII. Flutter Analysis After Model Tuning

Typical *V-g* and *V-ω* curves from the matched flutter analysis at Mach 0.82 after model tuning are given in Fig. 13. The same 3% structural damping value is used for flutter speed computation. In Fig. 13, we can observe a steeper merging behavior for the first bending and torsion modes after model tuning. It is important for the safety of flight that the model tuning results predict a more sudden, rather than a more gradual, flutter onset.

The results of the matched flutter analysis before and after model tuning are summarized in Tables 2 and 5. The modal participation factors in Table 5 indicate that the first three modes have more than a 95% contribution to the first flutter mode before model tuning and more than a 99% contribution after model tuning. The second mode,

Table 5 Modal participation factors before and after model tuning

Mode	Frequency, Hz	Modal participation factors before model tuning, %							
		Mach = 0.60		Mach = 0.75		Mach = 0.82		Mach = 0.95	
1	17.60	68.1		72.9		75.0		79.7	
2	23.26	22.2	95.5[a]	18.3	96.2[a]	16.8	96.6[a]	13.6	97.6[a]
3	93.99	5.2		5.0		4.8		4.3	
Mode	Frequency, Hz	Modal participation factors after model tuning, %							
		Mach = 0.60		Mach = 0.75		Mach = 0.82		Mach = 0.95	
1	17.45	5.0		8.2		10.7		22.6	
2	43.72	93.8	99.7[a]	90.0	99.6[a]	87.2	99.5[a]	71.4	96.4[a]
3	83.66	0.9		1.4		1.6		2.4	

[a]These are the sum of modes 1, 2, and 3 for each Mach number

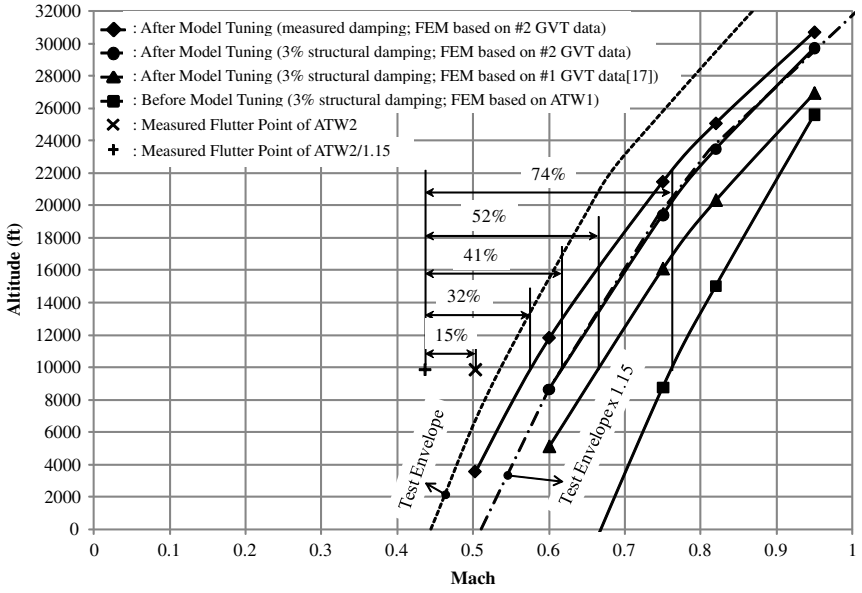

Fig. 14 Flutter boundary before and after model tuning.

Table 6 Required flutter margins for different types of structural dynamic models

Flutter boundaries	Flutter margins
Measured/1.15 (= V_d)	0%
Measured (=1.15 V_d)	15%
FEM; after model tuning; based on #2 GVT data; with measured damping	32%
FEM; after model tuning; based on #2 GVT data; with 3% structural damping	41%
FEM; after model tuning; based on #1 GVT data; with 3% structural damping	52%
FEM; before model tuning; with 3% structural damping	74%

which has the maximum frequency difference before model tuning as shown in Table 1, becomes more than 94% of the modal participation after model tuning at Mach 0.60. Therefore, the second mode after tuning becomes the dominant mode for the primary flutter mode. The resulting flutter speed difference due to model uncertainty was also a maximum at Mach 0.60, as shown in Table 2. Table 2 shows that the flutter speed difference varies from 33.8% at Mach 0.60 to 9.6% at Mach 0.95. As shown in Tables 2 and 5 after model tuning, the modal participation of the second mode, which is the dominant mode, decreased when Mach number increased; the differences in flutter speed due to uncertainty also decreased when Mach number increased.

Flutter boundaries of the ATW2, before and after model tuning, are compared with the flight envelopes as shown in Fig. 14. The dash line represents the ATW2 test envelope that is planned for flight, and the dash-dot line is the 15% margin of the ATW2 test envelope. This 15% margin line was designed to match the numerical flutter boundaries computed using the updated FE model with the 3% structural damping. The solid line with the square marker was the flutter boundary before model tuning, and the solid line with triangle marker was obtained from the [17]. The solid line with the diamond and circle markers represent flutter boundaries after model tuning using measured and 3% structural damping, respectively. Measured flutter point of the ATW2 is also shown in Fig. 14.

Finally, required flutter margins for the safety of flight were computed and summarized in Table 6. Note that the 32–52% of flutter margins are required with the test-validated structural dynamic models. In the case of the analytical FE model validated with the first GVT data [17], frequency error for the first mode, the most important mode for the first flutter mode, was slightly in violation of the military specification [14,15], 3.19% error instead of less than 3.00% error. However, this small violation causes more than 10% difference in flutter margin. Three percent structural damping for the flutter speed computation was acceptable as shown in Table 6. The difference in flutter margin was less than 9%, 41% minus 32%.

IX. Conclusions

This paper describes the reduced uncertainty procedures for the ATW2, which was developed at the NASA Dryden Flight Research Center to demonstrate flutter and advanced aeroelastic test techniques. Modeling uncertainties can be reduced through the tuning of the FE model using the NASA DFRC's object-oriented MDAO tool.

After tuning the FE model, the frequency differences between GVT and analytical results are within 3% and the off-diagonal terms of the orthonormalized mass matrix are within 10%, satisfying the military standards. Excellent mode shape correlations were also achieved through the high MAC value (greater than 95%).

For the flutter certification, if a structural dynamic model and an unsteady aerodynamic model are both test validated, a 15% flutter margin in the military specification can be used. If only the structural dynamic model is test validated, the flutter margin should be 37–52% in the case of the ATW2. Future work should focus on developing an unsteady aerodynamic model tuning methodology for precise flutter prediction during flight test.

Acknowledgment

This object-oriented multidisciplinary design, analysis, and optimization tool development was supported mainly by the Aeronautics Research Mission Directorate Subsonic Fixed Wing project and partly by the Aeronautics Research Mission Directorate Supersonics project under the Fundamental Aeronautics program.

References

[1] Lind, R., Voracek, D., Truax, R., Doyle, T., Potter, S., and Brenner, M., "A Flight Test to Demonstrate Flutter and Evaluate Flutterometer," *The Aeronautical Journal*, Vol. 107, No. 1076, Oct. 2003, pp. 577–588.

[2] Friswell, M. I., and Mottershead, J. E., *Finite Element Model Updating in Structural Dynamics*, Kluwer Academic Publishers, Norwell, MA, 1995.

[3] Pak, C.-G., "Finite Element Model Tuning Using Measured Mass Properties and Ground Vibration Test Data," *ASME Journal of Vibration and Acoustics*, Vol. 131, No. 1, Feb. 2009. doi: 10.1115/1.2981092.

[4] Pak, C.-G., and Li, W., "Multidisciplinary Design, Analysis and Optimization Tool Development Using a Genetic Algorithm," *Proceedings of the 26th Congress of International Council of the Aeronautical Science*, Anchorage, AL, 2008, www.icas-proceedings.net/ICAS2008/PAPERS/186.PDF [accessed April 2011].

[5] DOT Design Optimization Tools User's Manual Version 5.0., Vanderplaats Research & Development, Inc., 2001.

[6] Vanderplaats, G., *Numerical Optimization Techniques for Engineering Design*, 3rd ed., Vanderplaats Research & Development, Inc., Colorado Springs, CO, 2001.

[7] Charbonneau, P., and Knapp, B., *A User's Guide to PIKAIA 1.0*, National Center for Atmospheric Research, Boulder, CO, 1995.

[8] EI-Borgi, S., Neifar, M., Cherif, F., Choura, S., and Smaoui, H., "Modal Identification, Model Updating and Nonlinear Analysis of a Reinforced Concrete Bridge," *Journal of Vibration and Control*, Vol. 14, No. 4, 2008, pp. 511–530. doi:10.1177/1077546307079788

[9] Yeniay, Ö., "Penalty Function Methods for Constrained Optimization Using Genetic Algorithms," *Mathematical and Computational Applications*, Vol. 10, No. 1, 2005, pp. 45–56.

[10] Lung, S.-F., and Pak, C.-G., "Structural Model Tuning Capability in an Object-Oriented Multidisciplinary Design, Analysis and Optimization Tool," *Proceedings of the 26th Congress of International Council of the Aeronautical Sciences*, Anchorage, AL, 2008, www.icas-proceedings.net/ICAS2008/PAPERS/185.PDF [accessed April 2011].

[11] Herrera, C., and Pak, C.-G., "Build-up Approach to Updating the Mock Quiet Spike Beam Model," *Proceedings of the 48th AIAA/ASME/ASCE/AHS/ASC Structures, Structural Dynamics, and Materials Conference*, AIAA Paper 2007-1776, 2007.

[12] O'Callahan, J. C., "A Procedure for an Improved Reduced System (IRS) Model," *Proceedings of the 7th International Modal Analysis Conference*, Las Vegas, NV, Jan. 1989, pp. 17–21.

[13] O'Callahan, J. C., Avitabile, P., and Riemer, R., "System Equivalent Reduction Expansion Process," *Proceedings of the 7th International Modal Analysis Conference*, Las Vegas, NV, Vol. 1, 1989, pp. 29–37.

[14] Military Standard, "Test Requirements for Launch, Upper-Stage, and Space Vehicles," MIL-STD-1540C Section 6.2.10, Sept. 1994.

[15] Norton, W. J., "Structures Flight Test Handbook," U.S. Air Force Flight Test Center TIH-90-001, Nov. 1990.

[16] Lung, S.-F., and Pak, C.-G., "Updating Finite Element Model of the Aerostructures Test Wing with Ground Vibration Test Data," NASA TM-2009-214646.

[17] Pak, C.-G., and Lung, S.-F., "Reduced Uncertainties in the Flutter Analysis of the Aerostructures Test Wing," *Proceedings of the 27th Congress of International Council of the Aeronautical Science*, Nice, France, 2010, www.icas-proceedings.net/ICAS2010/PAPERS/072.PDF [accessed April 2011].

[18] Reymond, M., and Miller, M., "MSC/NASTRAN Quick Reference Guide version 69," The MacNeal Schwendler Corporation, 1996.

[19] ZAERO User's Manual ver. 8.2, ZONA Technology, Inc., March 2008.